Article type: Full Papers

Title: Asymmetric Transmission and Wavefront Manipulation Towards Dual-frequency Meta-holograms

Qirui Sun[†,‡,§], Zuojun Zhang[†,§], Yijia Huang[†,‡], Xiaoliang Ma[†], Mingbo Pu[†], Yinghui Guo[†], Xiong Li[†] and Xiangang Luo*,[†]

[†]State Key Laboratory of Optical Technologies on Nano-Fabrication and Micro-Engineering, Institute of Optics and Electronics, Chinese Academy of Sciences, P. O. Box 350, Chengdu 610209, China

[‡]School of Optoelectronics, University of Chinese Academy of Sciences, Beijing 100049, China

§These authors contributed equally.

* Corresponding Author: lxg@ioe.ac.cn

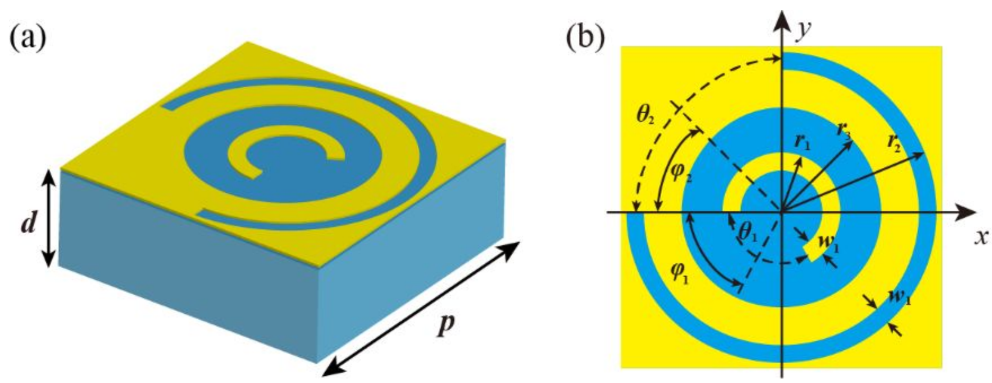

Figure S1. The schematic image of the single-layered unit cell which is obtained by removing the gratings and upper dielectric layer of the tri-layered unit cell in Figure 2(a). (a) 3D view of the unit cell. (b) Top view of the unit cell. The corresponding parameters are the same as the tri-layered one.

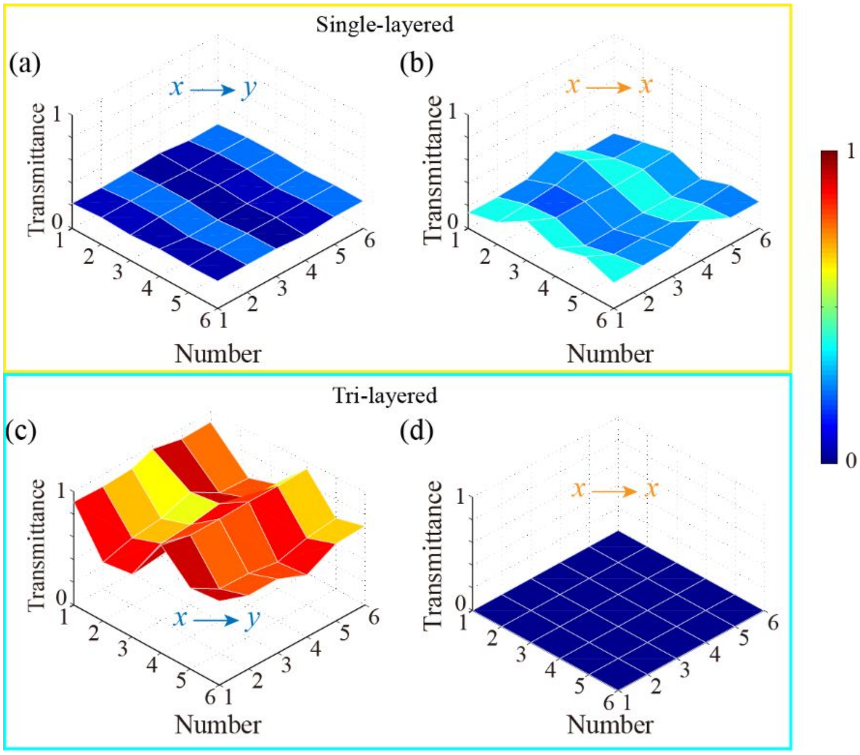

Figure S2. The transmittance of cross- and co-polarized EM waves at dual frequencies. (a), (b) The transmittance of cross- and co-polarized EM waves for single-layered unit cell. (c), (d) The corresponding results for tri-layered unit cell. The conversion efficiency of the tri-layered one is 3 and 7.5 times higher than the single-layered counterpart.

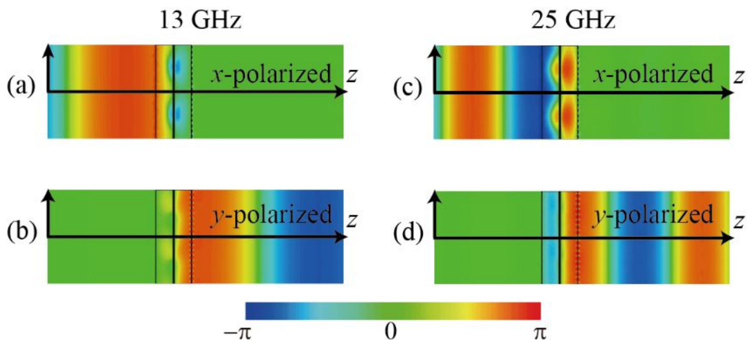

Figure S3. The electric field distributions of the proposed tri-layered unit cell under the incidence of *x*-polarized EM waves. (a), (b) The *x*- and *y*-polarized components of the EM waves at 13 GHz, respectively. (c), (d) The *x*- and *y*-polarized components of the EM waves at 25 GHz, respectively. Obviously, the incident *x*-polarized EM waves can be efficiently converted to their cross-polarized counterparts while the co-polarized EM waves can hardly transmit the unit cell.

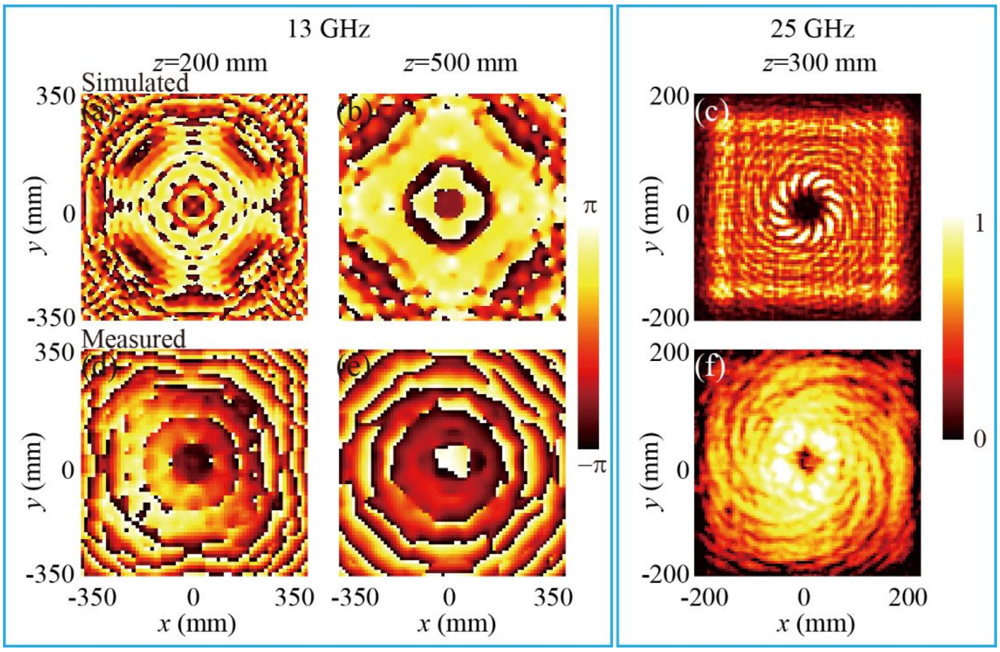

Figure S4. (a-b) Simulated and (d-e) measured phase distributions at 13 GHz at different distances from the metasurface. (c) Simulated and (f) measured amplitude distributions at 25 GHz.

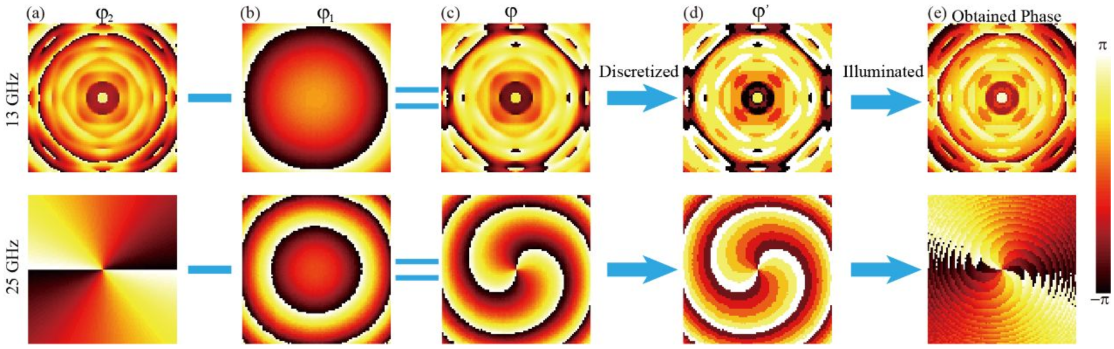

Figure S5. The compensation process for the holograms. Firstly, the phase distributions of the horn antenna were recorded as φ_1 (b) by employing the scanning field system at a distance of *d*=1 m at dual frequencies. Then, the encoded phase (c) in the metasurface is obtained by $\varphi=\varphi_2-\varphi_1$, where φ_2 (a) is the desired phase for meta-holograms. Finally, φ is discretized to six levels that are implemented by the proposed unit cells as φ' (d). (e) The obtained phase distributions when illuminated by the horn antenna.

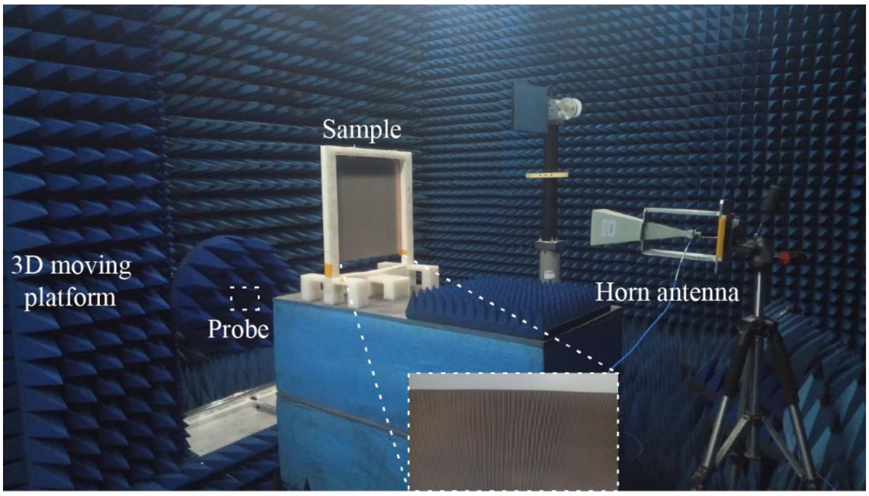

Figure S6. The schematic image of the testing system. The EM waves emitted by the horn antenna can be received by the waveguide probe. The probe is fixed on a 3D moving platform that can achieve point-to-point scanning in the transmitted field. The inset is the zoom-in picture of the fabricated sample. The white dotted square is the location of the waveguide.

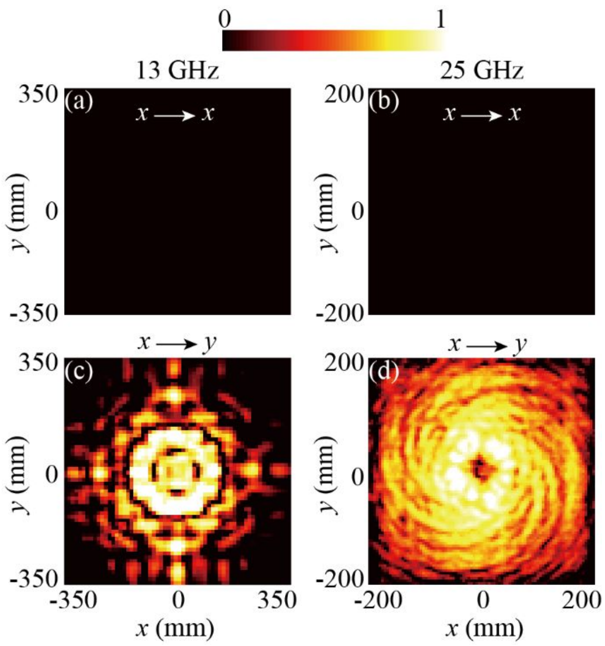

Figure S7. The measured transmitted co- and cross-polarized amplitudes under x-polarized incidence. (a), (b) The co-polarized transmitted field under dual frequencies. (c), (d) The cross-polarized transmitted field under dual frequencies.

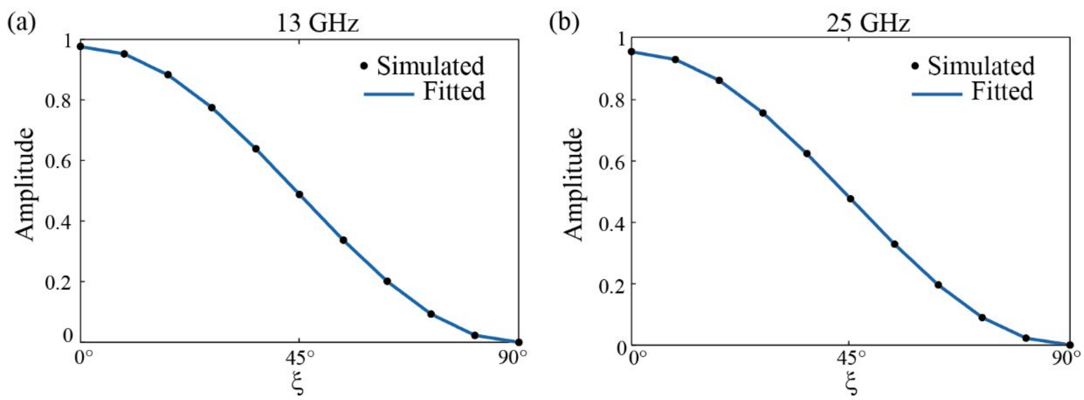

Figure S8. The transmission amplitude at various incident polarization angles at (a) 13 GHz and (b) 25 GHz. Both results (black dots) can be well fitted by a cosine curve (blue solid lines) that indicate the transmitted amplitude can be controlled by the incident polarizations.

Section S1. The detailed process for constructing the holograms

The three dimensional hologram at 13 GHz is obtained by the point-source algorithm and the original images are given in Figure S1. To obtain the needed phase distributions, each point on the image plane is treated as a point source and its corresponding phase distribution in the metasurface can be calculated by vectorial diffraction theory. The encoded phase is the superposition of phase distributions of all points.

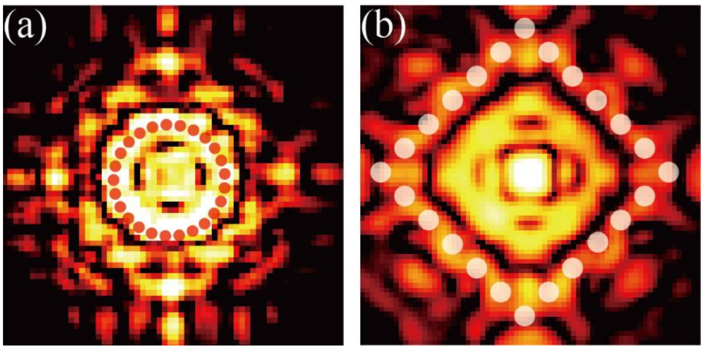

Figure S9. The original images at 13 GHz with red dots (a) and at 25 GHz (b) with white dots. The background in each figure is the measured result.

The desired phase distribution for vortex beam generation at 25 GHz is based on

$$\Phi(x, y) = l\varphi(x, y) \tag{1}$$

where l is the topological charge and $\varphi(x, y)$=arctan(y/x) is the azimuthal angle.

Table S1. The geometries of the designed unit cells.

i \ j		1	2	3	4	5	6
1	θ_1 (deg)	75	140	100	75	140	100
	φ_1 (deg)	-45	45	45	45	-45	-45
	r_1 (mm)	0.8	0.6	0.7	0.8	0.6	0.7
	θ_2 (deg)	70	70	70	70	70	70
	φ_2 (deg)	-45	-45	-45	-45	-45	-45
	r_2 (mm)	1.95	1.95	1.95	1.95	1.95	1.95
2	θ_1 (deg)	75	140	100	75	140	100
	φ_1 (deg)	-45	45	45	45	-45	-45
	r_1 (mm)	0.8	0.6	0.7	0.8	0.6	0.7
	θ_2 (deg)	55	55	55	55	55	55
	φ_2 (deg)	-45	-45	-45	-45	-45	-45
	r_2 (mm)	1.95	1.95	1.95	1.95	1.95	1.95
3	θ_1 (deg)	75	140	100	75	140	100
	φ_1 (deg)	-45	45	45	45	-45	-45
	r_1 (mm)	0.8	0.6	0.7	0.8	0.6	0.7
	θ_2 (deg)	115	115	115	115	115	115
	φ_2 (deg)	45	45	45	45	45	45
	r_2 (mm)	2.05	2.05	2.05	2.05	2.05	2.05
4	θ_1 (deg)	75	140	100	75	140	100
	φ_1 (deg)	-45	45	45	45	-45	-45
	r_1 (mm)	0.8	0.6	0.7	0.8	0.6	0.7

	θ_2 (deg)	70	70	70	70	70	70
	φ_2 (deg)	45	45	45	45	45	45
	r_2 (mm)	1.95	1.95	1.95	1.95	1.95	1.95
5	θ_1 (deg)	75	140	100	75	140	100
	φ_1 (deg)	-45	45	45	45	-45	-45
	r_1 (mm)	0.8	0.6	0.7	0.8	0.6	0.7
	θ_2 (deg)	5	5	5	5	5	5
	φ_2 (deg)	45	45	45	45	45	45
	r_2 (mm)	1.95	1.95	1.95	1.95	1.95	1.95
6	θ_1 (deg)	75	140	100	75	140	100
	φ_1 (deg)	-45	45	45	45	-45	-45
	r_1 (mm)	0.8	0.6	0.7	0.8	0.6	0.7
	θ_2 (deg)	115	115	115	115	115	115
	φ_2 (deg)	-45	-45	-45	-45	-45	-45
	r_2 (mm)	2.05	2.05	2.05	2.05	2.05	2.05